Information interactions between prefrontal cortex and hippocampus during performance of a spatial working memory task

Wei Zhang
Hebei University of Technology
Lei Guo (201521402001@stu.hebut.edu.cn)
Hebei University of Technology https://orcid.org/0000-0002-4253-206X
Dongzhao Liu
Hebei University of Technology
Guizhi Xu
Hebei University of Technology

Research Article

Keywords: spatial working memory, brain network, cross-frequency coupling, Granger causality, information interaction

Posted Date: March 17th, 2021

DOI: https://doi.org/10.21203/rs.3.rs-307683/v1

Abstract

Spatial working memory (SWM) refers to a short-term system for temporary manipulation of spatial information and requires the cooperation of multiple brain regions. Despite evidence that hippocampus (HPC) and prefrontal cortex (PFC) are involved in SWM, how PFC and HPC coordinate the neural information during SWM remains puzzling. In this study, local field potentials (LFPs) were recorded simultaneously from rat ventral HPC and medial PFC during SWM tasks. Then cross-frequency coupling algorithm was used as functional connectivity for construction of undirected networks; Grange causality algorithm was used as effective connectivity for construction of directed networks. Finally, information interactions across two brain regions were analyzed based on undirected and directed networks. Experimental results show that LFPs power in PFC and HPC both decreased over learning days and peaked before the reference point during SWM, moreover, LFPs mainly distributed in theta and gamma. From the undirected aspect, undirected PFC subnetwork and HPC subnetwork have the same effect on information transmission for SWM; the PAC between PFC-gamma and HPC-theta in undirected PFC-HPC network is related to SWM formation and contributes to information interactions between PFC and HPC. From the directed aspect, the effect of information transmission in directed HPC subnetwork is greater than PFC subnetwork; the enhancement of coordination between directed PFC and HPC subnetworks contributes to correct execution of SWM tasks; directed HPC→PFC network plays a predominant role in information interaction; with the increasing of learning days, PFC and HPC tend to be the causal sink and causal source of information flow.

Full Text

Due to technical limitations, full-text HTML conversion of this manuscript could not be completed. However, the manuscript can be downloaded and accessed as a PDF.

Figures

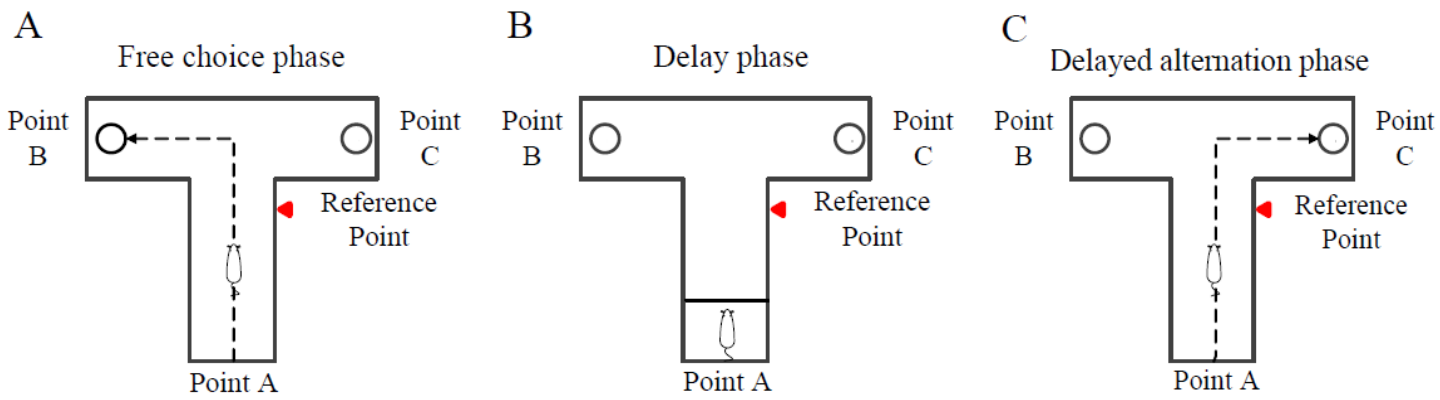

Figure 1

The schematic of the spatial delayed-alternation task on the T-maze. The T-maze consists of a starting arm, two target arms and a reference point of the behavioral selection. Rats were rewarded on the two target locations (Point B or C) and returned at the starting point (Point A) after a goal choice in one trial. Each trial of the task consisted of a free choice phase, delay phase and delayed alternation phase. A: The free choice phase. The rats can get reward by entering into either of target arms. B: The delay phase. The rats need to return to the Point A autonomously and wait for 10 seconds after a free choice run. C: The delayed alternation phase. The rats need to enter into the opposite arm to get food reward.

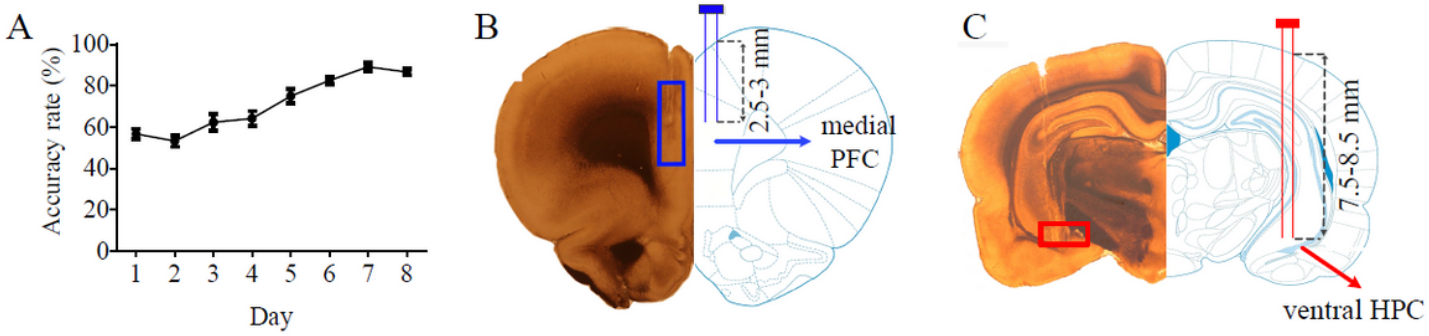

Figure 2

Behavioral performance and histology. A: The behavioral accuracy rate of the SWM training varied with days. The abscissa represents the learning days, and the ordinate represents the accuracy rate of the spatial delayed-alternation task. The accuracy rate increased significantly across the learning days (10 rats, one-way ANOVA: $F(7,40) = 21.26$, **** $P < 0.0001$). B: Histological verification of the recording sites in the medial PFC. C: Histological verification of the recording sites in the ventral HPC.

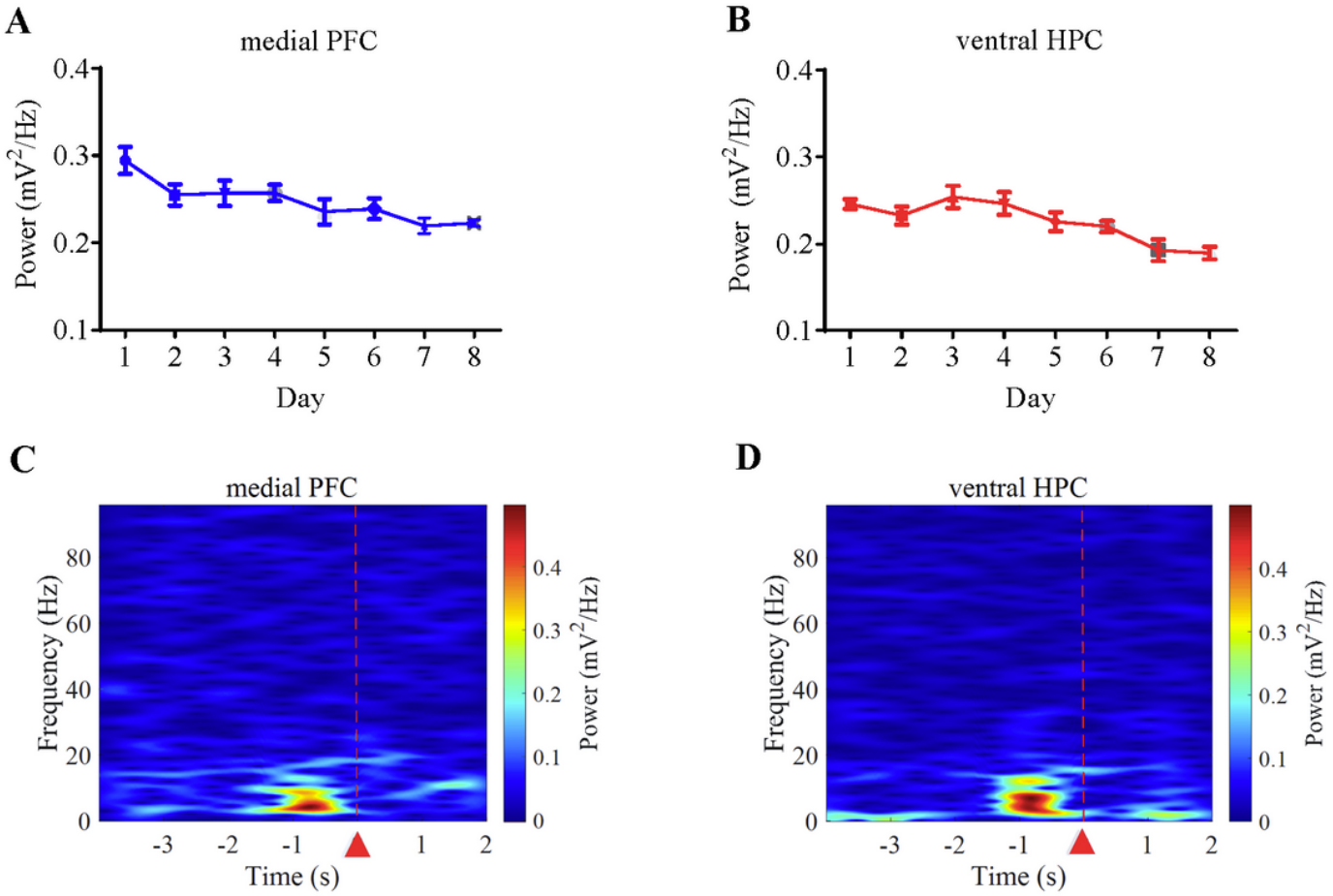

Figure 3

The dynamic changes of the LFPs in the medial PFC and ventral HPC (10 rats, 400 trials). A: The macro changes of the LFPs in the medial PFC over learning days. The LFPs in a trial were extracted from 2 seconds before the reference point to the rats' selection action in the delayed alternation phase. The LFPs power in the medial PFC decreased with an increase of days (one-way ANOVA, $F(7,42) = 3.838$, ** $P < 0.01$). B: The macro changes of the LFPs in the ventral HPC over learning days. The LFPs power in the ventral HPC decreased with an increase of learning days (one-way ANOVA, $(7,42)$ $F = 5.328$, *** $P < 0.001$). C: Time-frequency power spectrum analysis of LFPs in the medial PFC during delayed alternation phase. The abscissa represents the time over the delayed alternation phase, the red triangle represents the reference point of selection; the ordinate represents the LFPs frequency; the colorbar represents the LFPs power. D: Time-frequency power spectrum analysis of LFPs in the ventral HPC during delayed alternation phase.

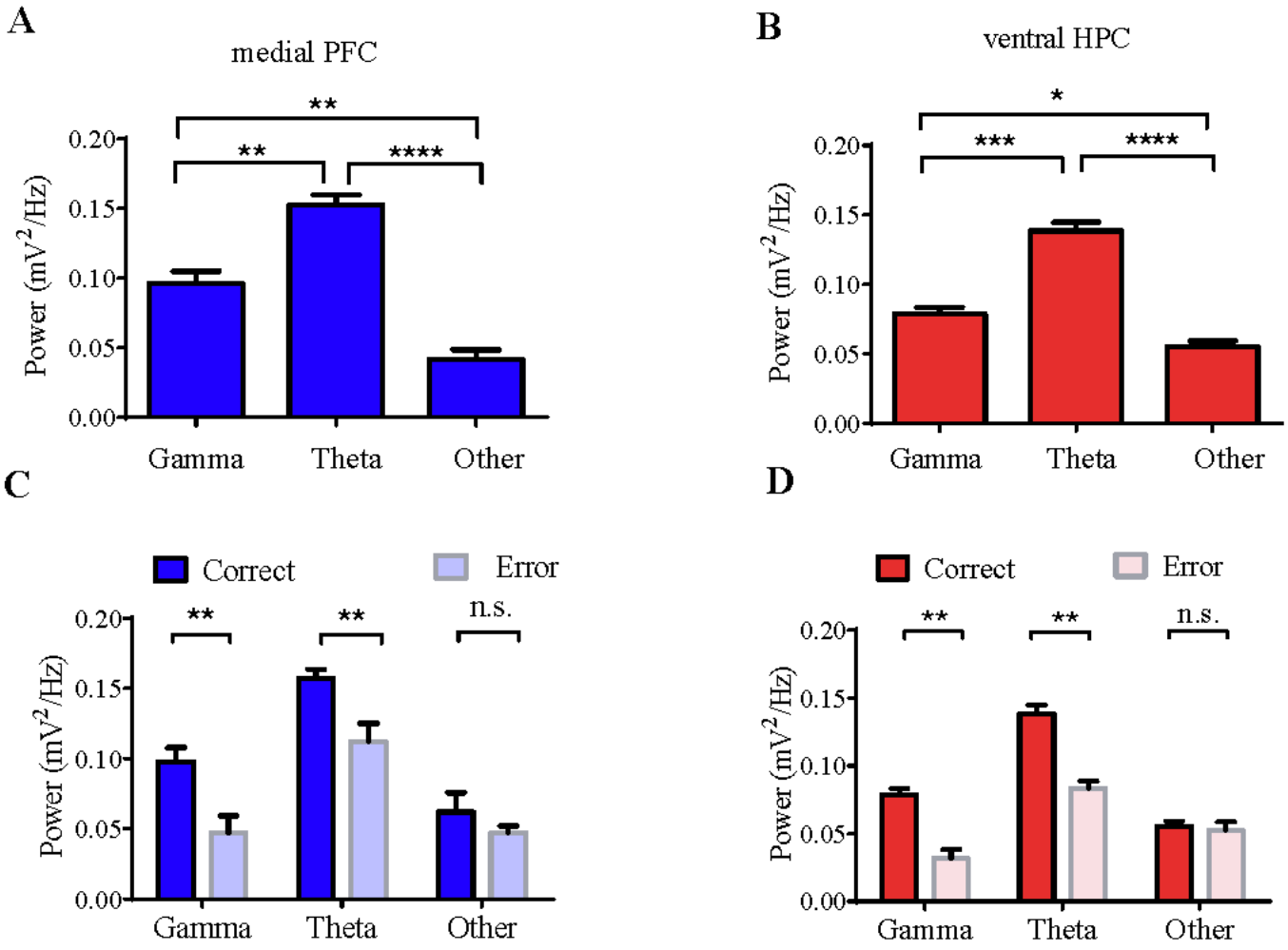

Figure 4

The distribution of the frequency bands of LFPs during SWM. In order to extract the characteristic frequency band of the LFPs for SWM, we calculated 300 trails from 10 rats when they have learned the SWM tasks. The LFPs during SWM state in a trial were extracted from 2 seconds before the reference point to the rats' selection action in the delayed alternation phase. A: The comparison of the power in theta (4-12 Hz), gamma (30-120 Hz) and other frequency bands in the medial PFC. The theta power in the medial PFC was significantly higher than gamma and other frequency bands, in addition, the gamma power was significantly higher than other frequency bands (one-way ANOVA and Bonferroni post-hoc test: ** $P < 0.01$, **** $P < 0.0001$). B: The comparison of the power in theta, gamma and other frequency bands in the ventral HPC. The theta power in the ventral HPC was significantly higher than gamma and other frequency bands, in addition, the gamma power was significantly higher than other frequency bands (one-way ANOVA and Bonferroni post-hoc test: * $P < 0.05$, *** $P < 0.001$, **** $P < 0.0001$). C: The comparison of different frequency bands in the medial PFC in correct and error trials (212 correct trials and 88 error trials). The power of theta and gamma in the medial PFC in correct trials were significantly higher than that in error trials. In addition, the power of other frequency band in correct and error trials had

no significance (independent sample t test, ** P < 0.01 , n.s.: no significance). D: The comparison of different frequency bands in the ventral HPC in correct and error trials. The power of theta and gamma in the ventral HPC in correct trials were significantly higher than that in error trials. In addition, the power of other frequency band in correct and error trials had no significance (independent sample t test, ** P < 0.01 , n.s.: no significance).

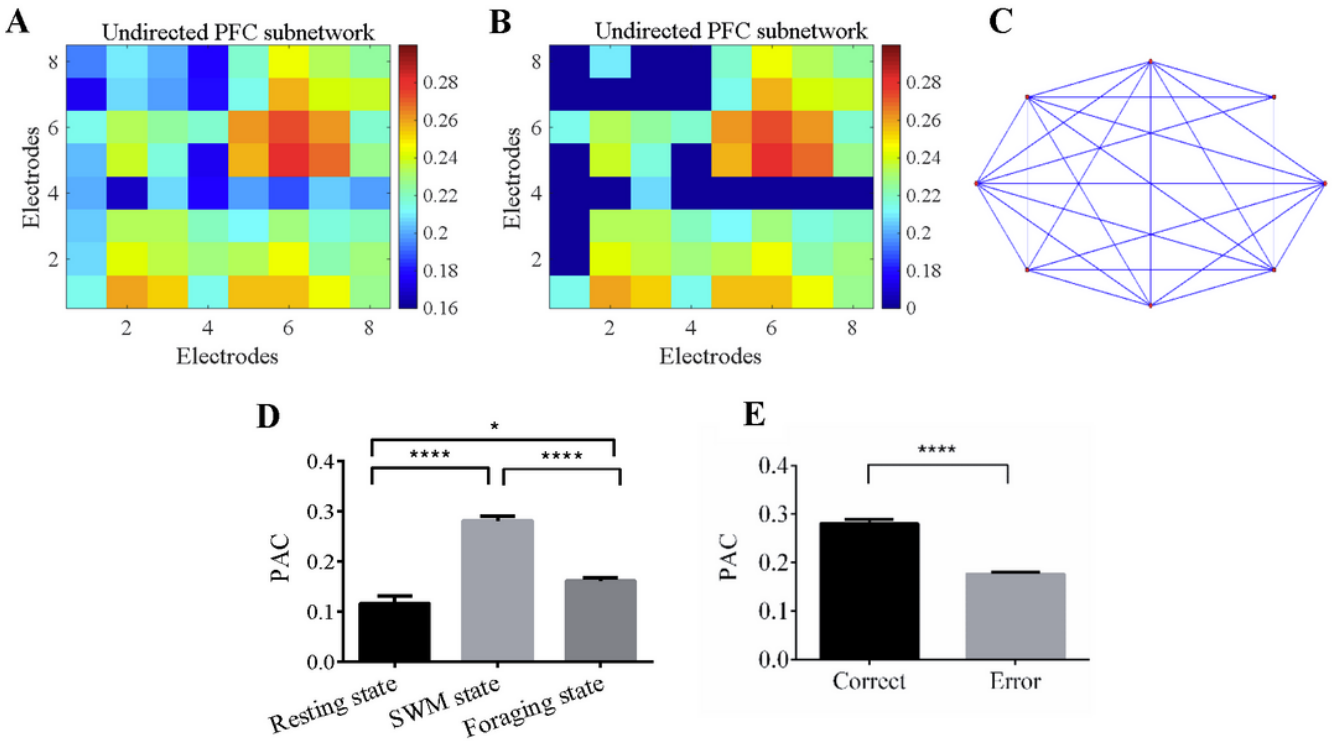

Figure 5

The information transmission in the undirected PFC subnetwork during SWM. We calculated 300 trails from 10 rats when they have learned the SWM tasks. A: The connectivity matrix of the undirected PFC subnetwork. The abscissa and ordinate represent the electrode index; the scaled color bar represents the PAC values of theta phase and gamma amplitude between electrodes. B: The weighted connectivity matrix of the undirected PFC subnetwork. C: The topology of the undirected PFC subnetwork. The nodes were 16-channel electrodes in the medial PFC and the connections between the nodes were the PAC values between the electrodes. D: The comparison of the PAC of the undirected PFC subnetwork in different behavioral states. The LFPs in the SWM state were extracted from 2 seconds before the reference point to the rats' selection action in the delayed alternation phase. The LFPs in the resting state were extracted from the delay phases. The LFPs in the foraging state were extracted after the rat's selection action in the delayed alternation phase. The PAC values in the SWM state were significantly higher than in the resting state and foraging state. In addition, the PAC values in the foraging state were significantly higher than in the resting states (one-way ANOVA and Bonferroni post-hoc test: **** P < 0.0001, * P < 0.05). E: The comparison of the PAC of the undirected PFC subnetwork in correct and error

trials (212 correct trials and 88 error trials). The PAC values in correct trials were significantly higher than in error trials (independent sample t test: **** P < 0.0001).

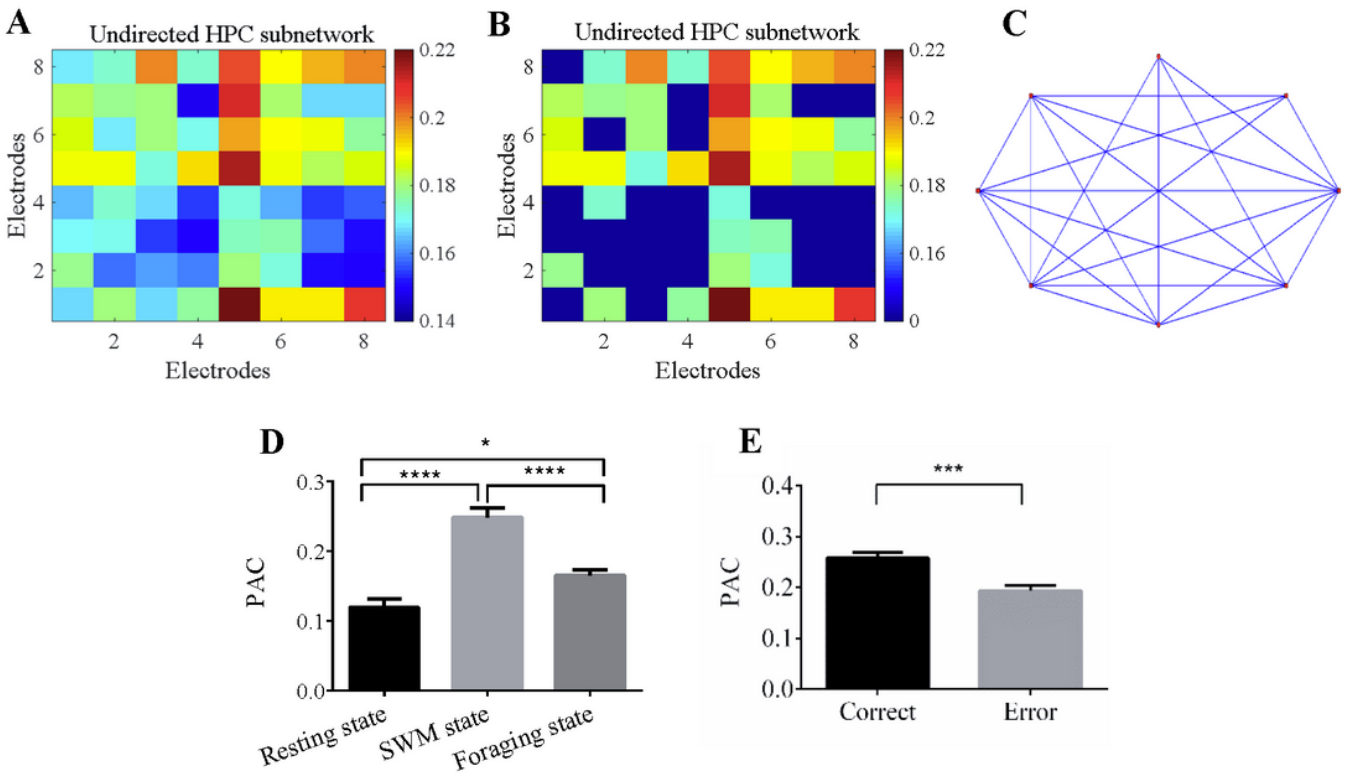

Figure 6

The information transmission in the undirected HPC subnetwork during SWM (10 rats, 300 trails). A: The connectivity matrix of the undirected HPC subnetwork. The abscissa and ordinate represent the electrode index; the scaled color bar represents the PAC values of theta phase and gamma amplitude between electrodes. B: The weighted connectivity matrix of the undirected HPC subnetwork. C: The topology of the undirected HPC subnetwork. The nodes were 16-channel electrodes in the ventral HPC and the connections between the nodes were the PAC values between the electrodes. D: The comparison of the PAC of the undirected HPC subnetwork in different behavioral states. The PAC values in the SWM state were significantly higher than in the resting state and foraging state. In addition, the PAC values in the foraging state were significantly higher than in the resting states (one-way ANOVA and Bonferroni post-hoc test: **** P < 0.0001, * P < 0.05). E: The comparison of the PAC of the undirected HPC subnetwork in correct and error trials (212 correct trials and 88 error trials). The PAC values in correct trials were significantly higher than in error trials (independent sample t test: *** P < 0.001).

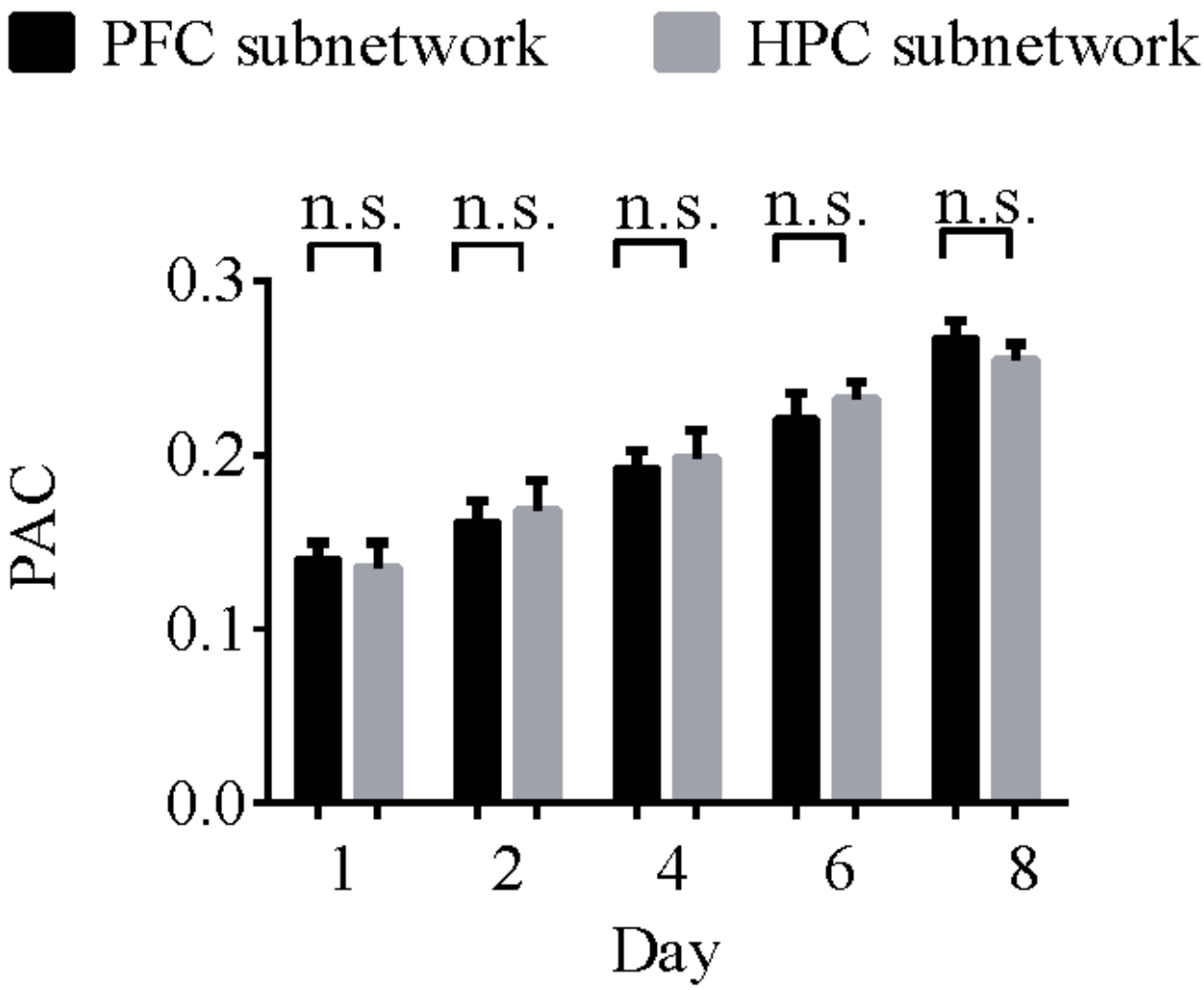

Figure 7

The comparison of the PAC in the undirected PFC subnetwork and HPC subnetwork over learning days. There was no significance for the PAC values in the PFC subnetwork and HPC subnetwork in different learning days (paired sample t test, n.s.: no significance).

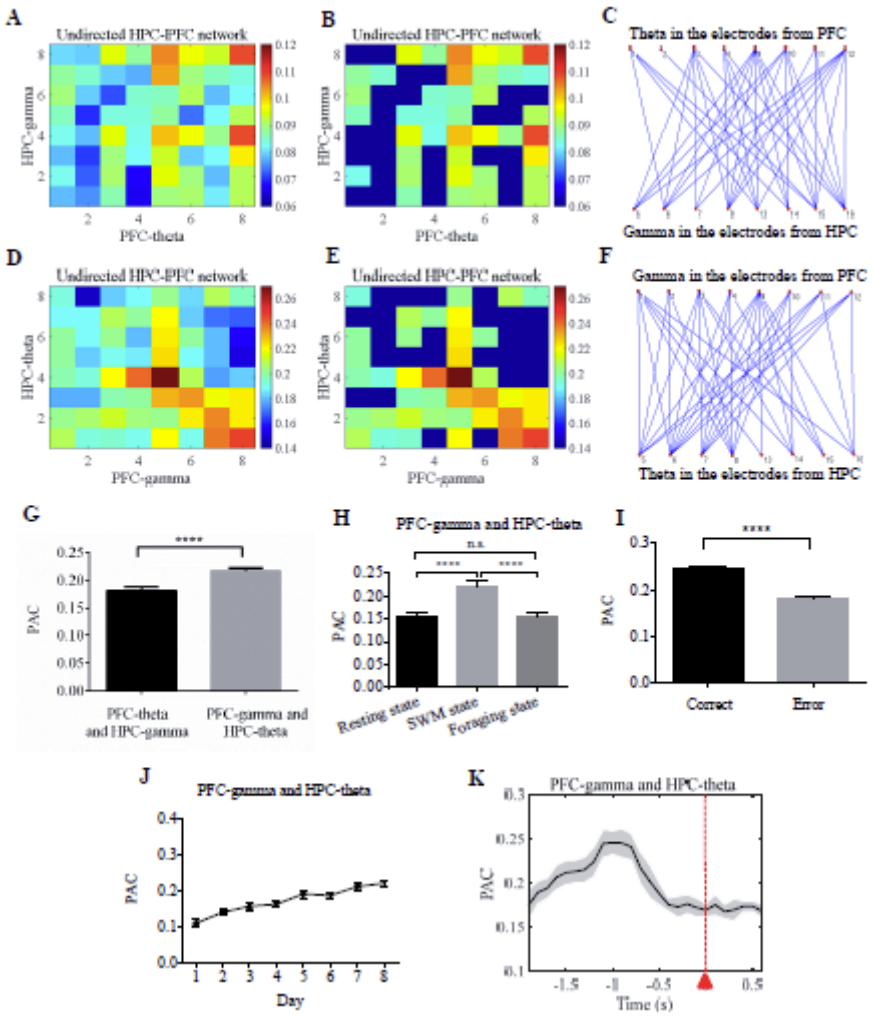

Figure 8

The information interaction in the undirected HPC-PFC network during SWM. A: The connectivity matrix of the undirected HPC-PFC network based on the PAC between theta phase in the PFC (PFC-theta) and gamma amplitude in the HPC (HPC-gamma). B: The weighted connectivity matrix of the undirected HPC-PFC network based on the PAC between PFC-theta and HPC-gamma. C: The topology of the first type of undirected HPC-PFC network. D: The connectivity matrix of the undirected HPC-PFC network based on the PAC between gamma amplitude in the PFC (PFC-gamma) and theta phase in the HPC (HPC-theta). E: The weighted connectivity matrix of the undirected HPC-PFC network based on the PAC between PFC-gamma and HPC-theta. F: The topology of the second type of undirected HPC-PFC network. G: The comparison of the two types of undirected HPC-PFC network. The PAC values in the second type of undirected HPC-PFC network were significantly higher than these in the first type of undirected HPC-PFC network (paired sample t test: **** $P < 0.0001$). H: The comparison of the PAC between PFC-gamma and HPC-theta in the undirected HPC-PFC network in different behavioral states. The PAC values in the SWM state were significantly higher than in the resting state and foraging state (one-way ANOVA and Bonferroni post-hoc test: **** $P < 0.0001$). I: The comparison of the PAC in correct trials and error trials. The PAC values in correct trials were significantly higher than in error trials (independent sample t test: **** $P < 0.0001$). J:

The change of the PAC between PFCgamma and HPC-theta in the undirected HPC-PFC network over learning days. The PAC increased significantly with an increasing of learning days (one-way ANOVA, (7,152) F □ 1.139 , **** P < 0.0001). K: The changes of the PAC between PFC-gamma and HPC-theta in the undirected HPC-PFC network during SWM state. The abscissa represents the time during SWM state and the red triangle represents the reference point. The PAC values peaked before the reference point during the SWM state.

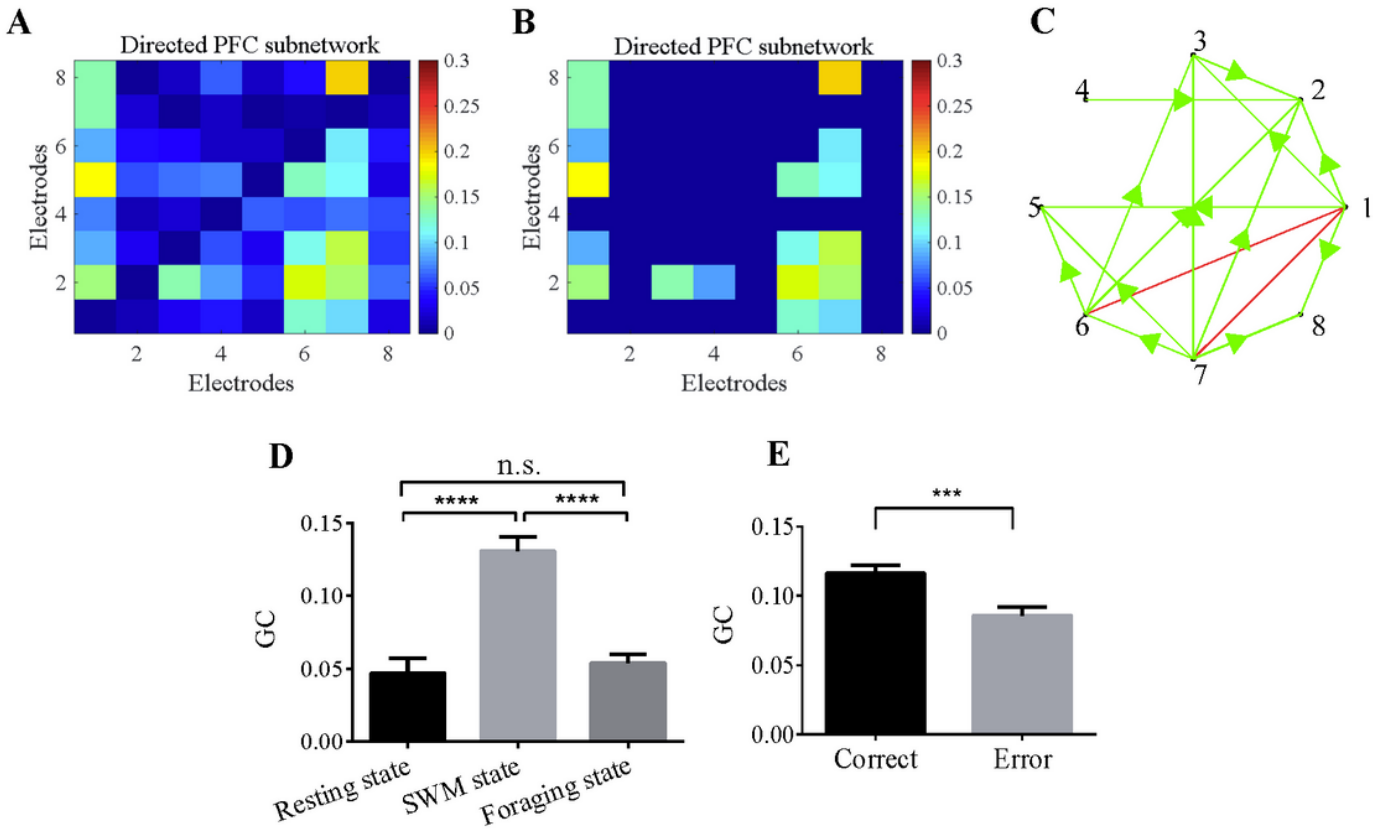

Figure 9

The information transmission in the directed PFC subnetwork during SWM. A: The connectivity matrix of the directed PFC subnetwork. The abscissa and ordinate represent the electrode index; the scaled color bar represents the GC values of electrodes. B: The weighted connectivity matrix of the directed PFC subnetwork. C: The topology of the directed PFC subnetwork. The nodes were 16-channel electrodes in the medial PFC and the connections between the nodes were the GC values of the electrodes. D: The comparison of the GC of the directed PFC subnetwork in different behavioral states. The GC values in the SWM state were significantly higher than in the resting state and foraging state (one-way ANOVA and Bonferroni post-hoc test: **** P < 0.0001). E: The comparison of the GC of the directed PFC subnetwork in correct and error trials (212 correct trials and 88 error trials). The GC values in correct trials were significantly higher than in error trials (independent sample t test: *** P < 0.001).

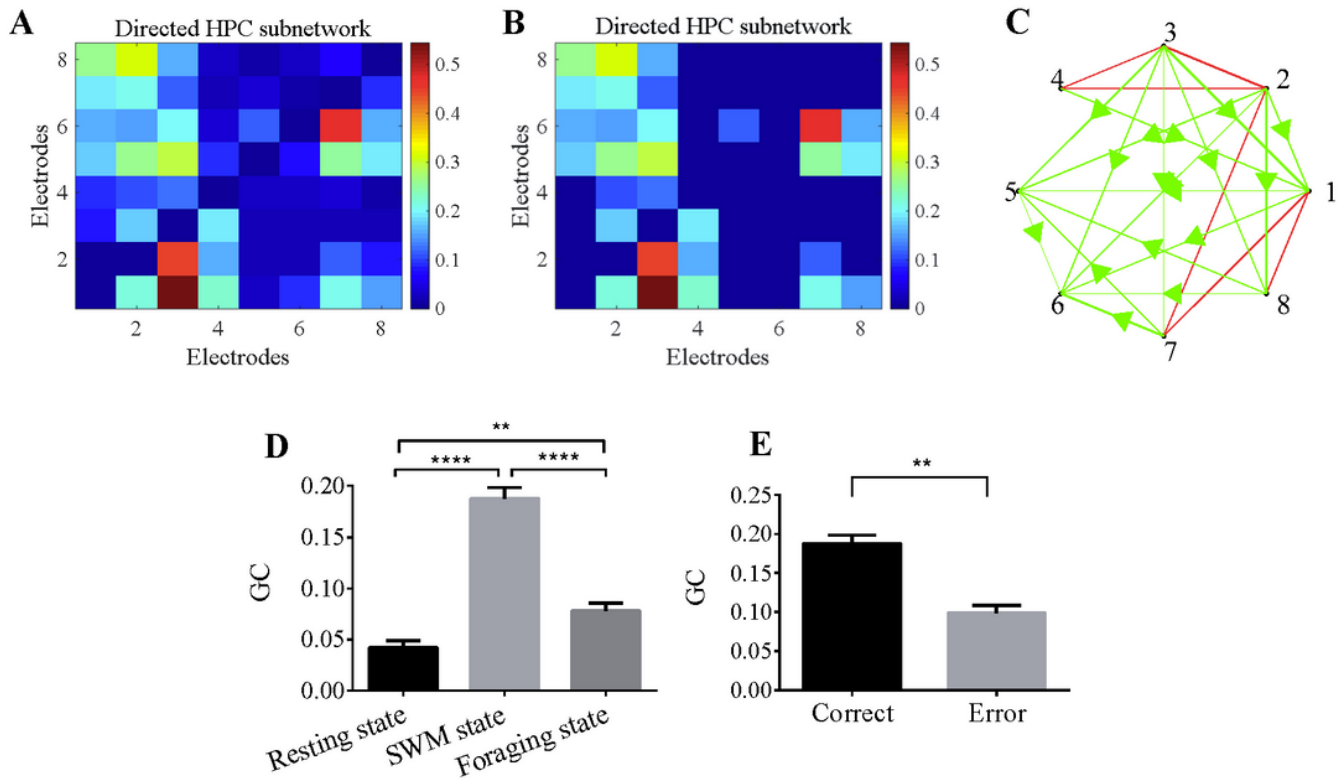

Figure 10

The information transmission in the directed HPC subnetwork during SWM. A: The connectivity matrix of the directed HPC subnetwork. B: The weighted connectivity matrix of the directed HPC subnetwork. C: The topology of the directed HPC subnetwork. The nodes were 16-channel electrodes in the ventral HPC and the connections between the nodes were the GC values of the electrodes. D: The comparison of the GC of the directed HPC subnetwork in different behavioral states. The GC values in the SWM state were significantly higher than in the resting state and foraging state. In addition, the GC values in the foraging state were significantly higher than these in the resting state (one-way ANOVA and Bonferroni post-hoc test: **** $P < 0.0001$, ** $P < 0.01$). E: The comparison of the GC of the directed HPC subnetwork in correct and error trials (212 correct trials and 88 error trials). The GC values in correct trials were significantly higher than in error trials (independent sample t test: ** $P < 0.01$).

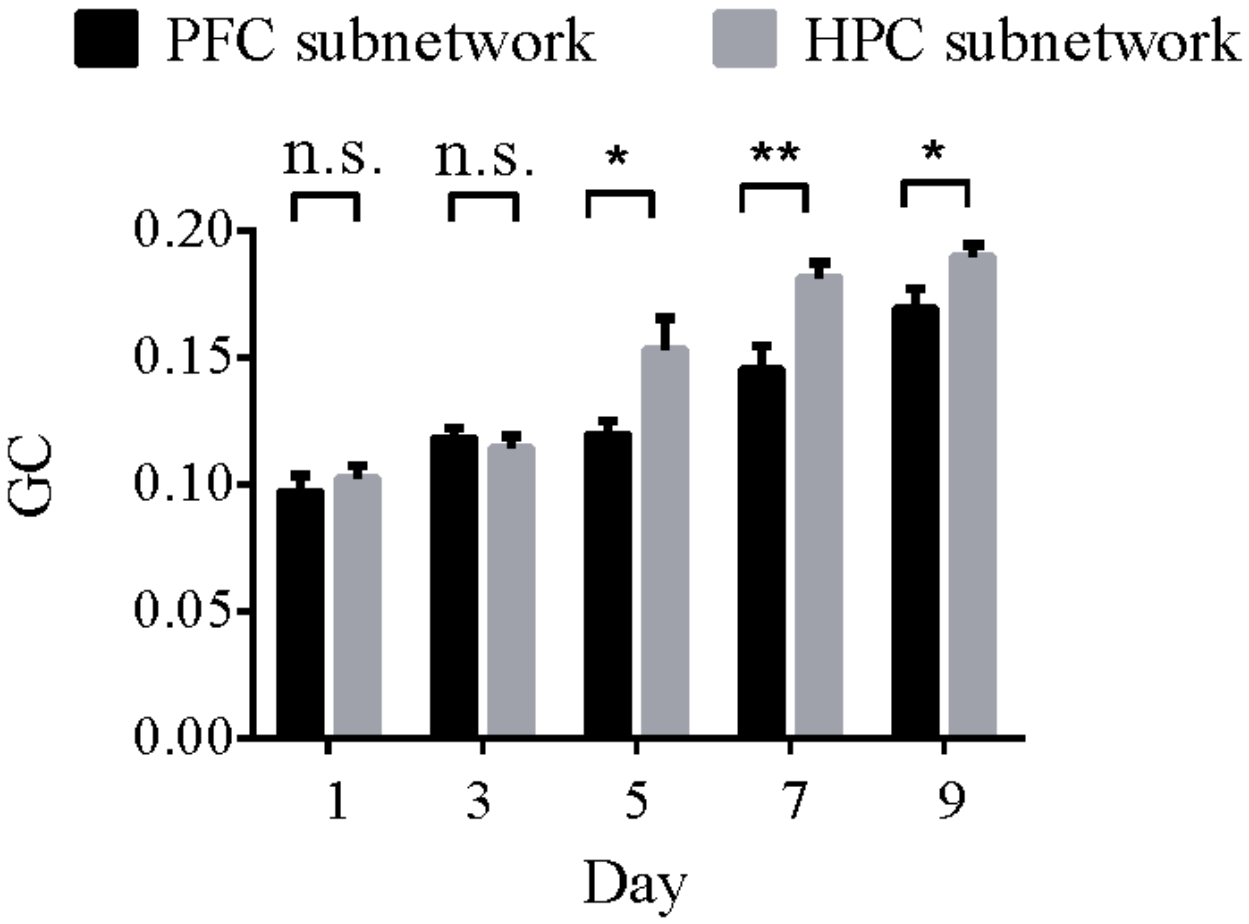

Figure 11

The comparison of the directed PFC subnetwork and HPC subnetwork over learning days. There was no significance for the GC values in the PFC subnetwork and HPC subnetwork in first and third days. The GC values in the HPC subnetwork were significantly higher than in the PFC subnetwork with an increasing of the learning days (paired sample t test, * $P < 0.05$, ** $P < 0.01$, n.s.: no significance).

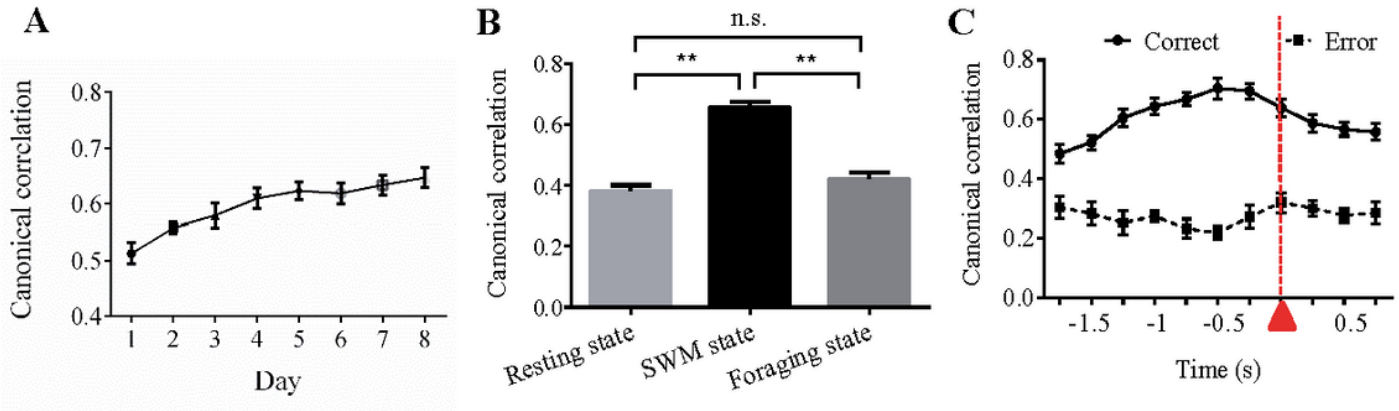

Figure 12

The coordination between directed PFC subnetwork and HPC subnetwork during SWM. A: The changes of the canonical correlation between directed PFC subnetwork and HPC subnetwork over learning days. The correlation between two subnetworks increased with an increasing of learning days (one-way ANOVA, F(7,86) 0.7498 , **** P < 0.0001). B: The comparison of the canonical correlation between two subnetworks in different behavioral states. The values of the canonical correlation in SWM state were significantly higher than in resting and foraging states (one-way ANOVA and Bonferroni post-hoc test: ** P < 0.01). D: The comparison of the changes of canonical correlation between two subnetworks during SWM state in correct and error trials. The abscissa represents the behavioral time during SWM; the solid line legend represents the dynamic changes of the correlation in correct trials; the dotted line legend represents the dynamic changes of the correlation in error trials. We used the two-way ANOVA of repeated measurements for statistical analysis. The behavioral time was set as the time factor and correct and error trials as the group factor. There was significance between correct and error trials in different behavioral time (group factor: * P < 0.05 ; time factor: ** P < 0.01). In correct trials, the correlation between two subnetworks increased and peak before the reference point (red triangle). While in error trials, there was no significant enhancement and the peak for the correlation.

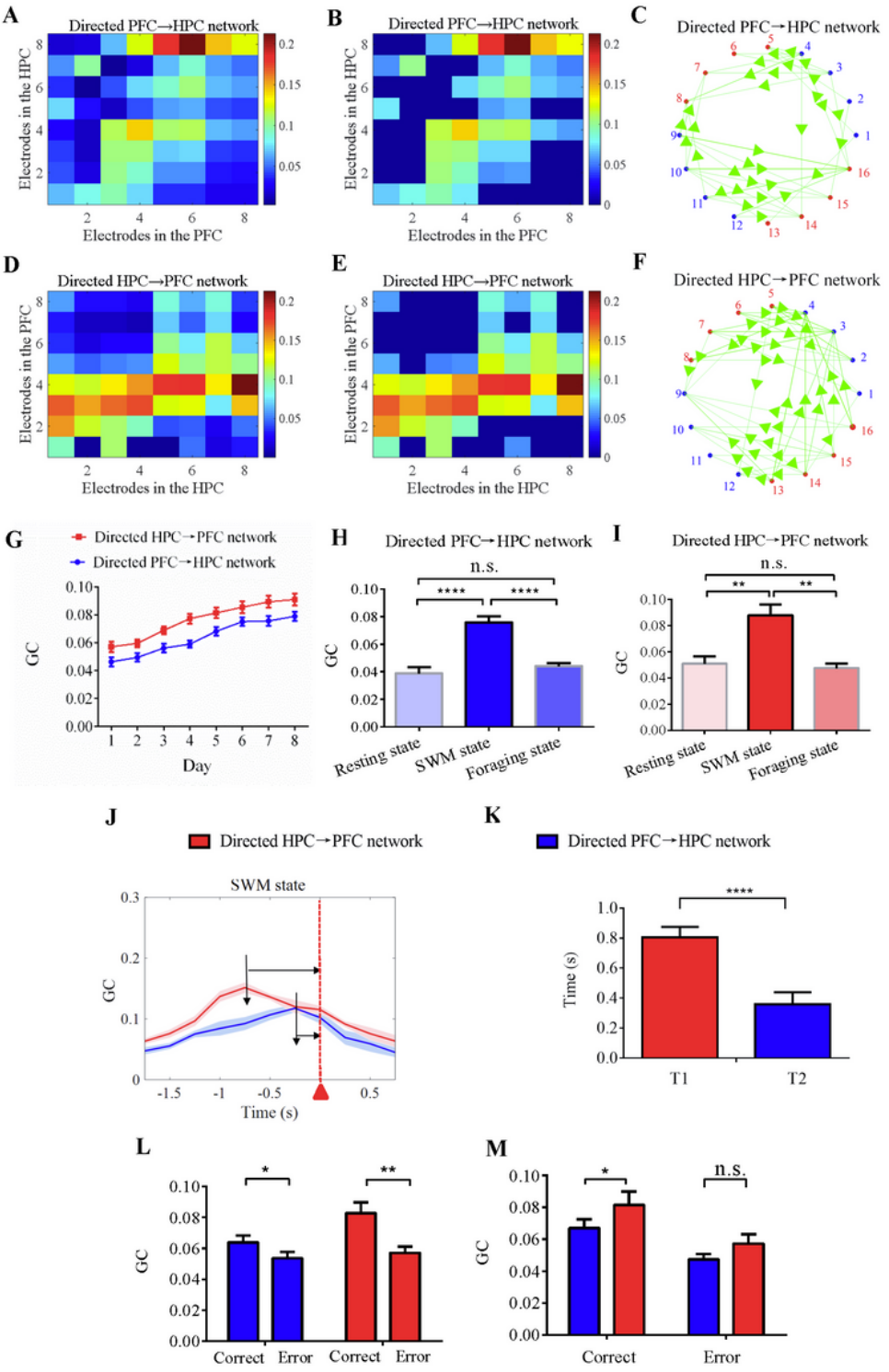

Figure 13

The information interaction in the bidirectional HPC-PFC networks during SWM. A: The connectivity matrix of the directed PFC→HPC network. B: The weighted connectivity matrix of the directed PFC→HPC network. C: The topology of the directed PFC→HPC network. D: The connectivity matrix of the directed HPC→PFC network. E: The weighted connectivity matrix of the directed HPC→PFC network. F: The topology of the directed HPC→PFC network. G: The changes of the GC in the directed PFC→HPC and

HPC→PFC networks over learning days. The GC values in the bidirectional networks both increased with an increasing of learning days (one-way ANOVA, ** P < 0.01 , *** P < 0.001). H: The comparison of the GC in the directed PFC→HPC network in different behavioral states. The GC values in the SWM state were significantly higher than in the resting state and foraging state (one-way ANOVA and Bonferroni post-hoc test: **** P < 0.0001). I: The comparison of the GC in the directed HPC→PFC network in different behavioral states. The GC values in the SWM state were significantly higher than in the resting state and foraging state (one-way ANOVA and Bonferroni posthoc test: ** P < 0.01). J: The changes of the GC in the bidirectional networks during SWM state. T1 is the time interval between the peak and reference point in the red curve; T2 is the time interval between the peak and reference point in the blue curve. The GC values in bidirectional networks both peaked before the reference point during the SWM state. Moreover, the GC values in the directed HPC→PFC network peaked prior to those in the directed PFC→HPC network. K: The comparison of the time intervals. T1 was significantly higher than T2 (paired sample t test: **** P < 0.0001). L: The comparison of the GC values in correct and error trials. The GC values in the bidirectional networks in correct trials were both significantly higher than in error trials (independent sample t test: * P < 0.05 , ** P < 0.01). M: The comparison of the GC values in bidirectional networks. In correct trials, the GC values in the directed HPC→PFC network were significantly higher than in the directed PFC→HPC networks; while in error trials, there was no significance for GC in the bidirectional networks (paired sample t test: * P < 0.05 , n.s.).

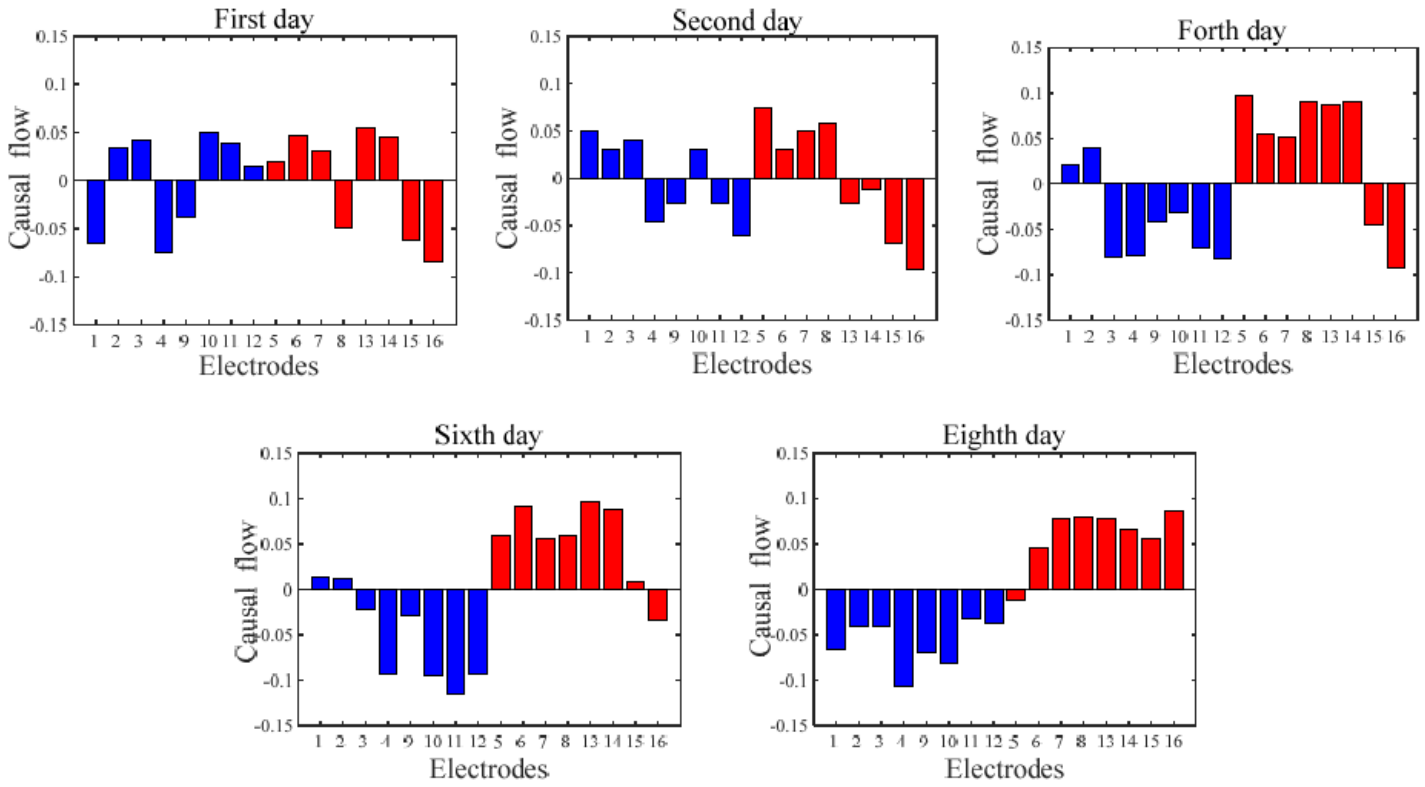

Figure 14

The information flow in the PFC and HPC brain regions during SWM in different learning days. The blue bars represent the electrodes in the PFC and the red bars represents the electrodes in the HPC. The

positive value of the causal flow indicates the electrode is the causal source; the negative value of the causal flow indicates the electrode is the causal sink. From first day to second day, there were positive and negative causal flow in the PFC and HPC, and the direction of the causal flow was inconsistent. With the increasing of learning days, the direction of causal flow in the PFC and HPC tended to be consistent. The causal flow in the PFC was negative, which indicates the PFC is the causal sink. While the causal flow in the HPC was positive, which indicates the HPC is the causal source.